INTERNATIONAL JOURNAL FOR NUMERICAL METHODS IN ENGINEERING
Int. J. Numer. Meth. Engng 2011; **85**:1390–1414
Published online 1 September 2010 in Wiley Online Library (wileyonlinelibrary.com). DOI: 10.1002/nme.3022

Coupling heat conduction and water–steam flow in a saturated porous medium

M. Muhieddine[1,2,*,†], É. Canot[1], R. March[2] and R. Delannay[3]

[1]*IRISA, Campus de Beaulieu, 35042 Rennes, France*
[2]*Archéosciences, UMR 6566, Campus de Beaulieu, 35042 Rennes, France*
[3]*IPR, UMR 6251, Campus de Beaulieu, 35042 Rennes, France*

SUMMARY

This paper is devoted to the simulation of water forced evaporation in a porous saturated medium in a 3D-axisymmetric domain by resolution of partial differential algebraic equations (PDAE) that are encountered in different engineering applications. The goal of this paper is an attempt to present effective realizations, in order to determine the minimal duration of burning for prehistoric occupations. This multidisciplinary work includes scientists in Mathematics, Physics and Archaeology. The model proposed here couples the heat conduction in a water saturated soil with the water steam flow in the medium. We propose an efficient and robust global numerical method, based on a method of lines and differential algebraic equations (DAE) solvers, combined with a Newton method using a powerful sparse linear solver. After a brief overview of classes for numerical techniques applied for moving boundary problems, the Apparent Heat Capacity method (AHC) is used, and in order to validate our codes, a comparison with experiments is done. Copyright © 2010 John Wiley & Sons, Ltd.

Received 25 November 2008; Revised 2 July 2010; Accepted 21 July 2010

KEY WORDS: phase change problem; gas flow in porous media; high performance computing; finite volume method; implicit ODE system; heat conduction

1. INTRODUCTION

Heat flow accompanied by a phase change occurs in many important practical problems. In particular, the heat diffusion in the ground saturated by water have pressed upon the attention to develop new methods for more precise representative simulations. Actually, the aim of this work is to present the applied mathematics used to study prehistoric fires. The goal is to determine the minimal duration of burning for the archaeological hearths in order to understand the ancient human behaviors related to the use of fire. In fact, the minimal duration of burning gives us an idea if the fire was used for cooking, to drive away the animals, etc. The idea is to apply a numerical model to calculate the heat conduction in porous soils subjected to intense heat from above in order to determine their minimal duration of burning. This particular geometry involves that the heat prevents the usual behavior of fluid in the ground, because the vapor ascends to the heated surfaces.

Subsequently, the mathematical model delineating our problems is described by a coupled system of moving boundary problems with phase changes and the convection phenomenon under a downward facing heated surface [1]. This work is of importance due to the inherent difficulties associated with the non-linearity of the interface conditions, the unknown locations of the moving boundaries (liquid/vapor interface) and the coupling with the non-linear convection problem.

*Correspondence to: M. Muhieddine, IRISA, Campus de Beaulieu, 35042 Rennes, France.
†E-mail: mohamad.muhieddine@irisa.fr

It should be mentioned that this problem has a wide application in many engineering fields, like the liquid–vapor phase change in an enclosed cavity. Indeed, water substance plays a very important role in science and industry. Reliable information for equilibrium thermodynamic and transport properties of water and steam (water substance) are mostly needed for engineering applications where heat transfer analysis is involved. In view of these facts, this paper presents a review of progress made in the past few decades on the formulation and the resolution of thermal conduction with phase-change phenomenon coupled with water steam flow.

Over the years, a number of related computational works have employed various techniques in the analysis of phase-change problems. Several important theoretical results on the existence, the uniqueness and the properties of classical solutions can be found [2, 3], but most of analytical solutions are for 1-D geometries with very particular boundary conditions [4, 5], and cannot be extended to multidimensional problems [6, 7]. Thus, many numerical schemes have been proposed to study transient heat conduction problems with phase change in one, two and three dimensions, but two schemes are predominant in the numerical analysis; the first one is referred to as the 'front-tracking method', in which the position of the moving front is determined at each time step [8], and must always correspond to a node or edges mesh. The use of this numerical method can usually eliminate the oscillations found by using the fixed grid method [9, 10], and allows for more precise solutions. These methods are poorly suited to multi-dimensional problems due to the implementation difficulties and the large computational cost.

The second scheme formulates the problem in such a way that the conditions on the moving phase front may be absorbed into new equations, and the problem is solved without explicit reference to the position of the internal boundary. This position is determined *a posteriori* when the solution is complete, using the isotherms at 100°C. Such a reformulation is based on the use of the heat enthalpy concept [9, 11–13]. The major problem with these schemes is the presence of oscillations in the solution. In addition, these schemes often require the use of algorithms to adjust the solution in order not to miss the absorption or the release of latent heat. The major advantage of these methods is that they are easily applicable to the phase-change problems.

Other publications related to the natural convection for better understanding of transport phenomena in geothermal energy systems can be found in [4, 14]. This problem is a real challenge from both modeling and computational standpoints. It has received much attention in the recent past and is still the subject of intensive ongoing research.

In fact, simulations of liquid–vapor flows coupled with heat flow accompanied by a phase change with realistic physical properties and large density ratio between the phases (≈ 1000) are still few in the literature. This is due to various modeling and numerical difficulties. Also, the numerical method for such problems needs to deal with incompressible (liquid) and compressible (vapor) flows in the same computational domain. This difficulty can be overcome using different computational sub-domains for the two-phases, but this approach is limited to small deformations of the interface.

The model developed in the present paper uses the AHC method to describe the phase-change phenomenon of the fluid (water) in the ground. The physical properties of the fluid (water/vapor) used in the calculation are temperature dependent; therefore, the problem is highly non-linear. Also, the compressibility of the created vapor coupled with the phase-change effects is significant too, yielding much more complex dynamics, that is why it is interesting to develop a numerical methodology to handle and solve this problem. Otherwise, a systematic study of the evaporation in the soil will be based on an experimental methodology definitely more general that allows the settling of innovative designs to facilitate the approach modeling and its validation.

We present here a unified framework for many numerical methods and we introduce a new formulation of a global approach using the power of differential algebraic equations (DAE) solvers. In the diffusion model, we assume that the porous medium is saturated by water. By adding the flow model, we get a coupled set of PDAE. There are various ways to discretize the diffusion operator, but we restrict this study to Eulerian approaches, for example by finite differences, finite-volume or finite element methods. Moreover, we consider a method of lines where space is first discretized, and the resulting semi-discrete system is then solved by an ordinary differential equation (ODE)

DOI: 10.1002/nme

(or DAE) solver depending on if we are dealing with coupled system or just the diffusion part. This excludes methods combining time and space discretizations. We also assume that the same discrete space is used for advection and diffusion, so that we get a discrete advection–diffusion equation. With these assumptions, the model is transformed into a set of DAE of finite dimension, where unknowns are in the discrete space.

Most of the used approaches in the literature differ by the numerical scheme used to discretize in time and by the numerical method used to solve the non-linear equations. Our approach uses an implicit scheme and a Newton method embedded in a DAE solver; the objective is to rely on the solver for controlling the time step, the order of the scheme, the updates of the Jacobian and the convergence of Newton iterations. In order to improve efficiency, we use sparse Jacobian matrix and sparse linear solver.

2. MATHEMATICAL FORMULATION

Consider a horizontal surface embedded in a water saturated porous medium as shown in Figure 1. The temperature of the surface facing downward is T_C, which is greater than the temperature of the medium T_∞ at an infinite depth.

To describe the evaporation of water in a soil, whether natural or forced, which involves very complex mechanisms we consider basic phenomena and to simplify the model, we adopt the following assumptions:

1. The solid phase (porous matrix) is composed of a single constituent that does not react with other constituents and does not dissolve. Its properties may vary in space.
2. Deformations of the solid phase are neglected.
3. The moisture is present mainly in the form of free water and does not react chemically with other constituents.
4. The dry front appears immediately at the open surface when the heating begins.
5. The phase-change temperature $T_v = 100°C$ (this is justified a posteriori because pressure variations are very small).

Also, there is thermal equilibrium between the liquid and vapor phases on the interface of phase change, which leads to an identical temperature for both phases on this interface.

Combarnous and Bories have derived a two-energy equation model for heat transfer within a unit volume of a porous medium [15]. For the fluid phase, they gave

$$\operatorname{div}(\lambda_f \operatorname{grad} T_f) - \operatorname{div}[(\rho C)_f V_f T_f] = \frac{\partial}{\partial t}[\phi(\rho C)_f T_f] + h(T_f - T_s) \tag{1}$$

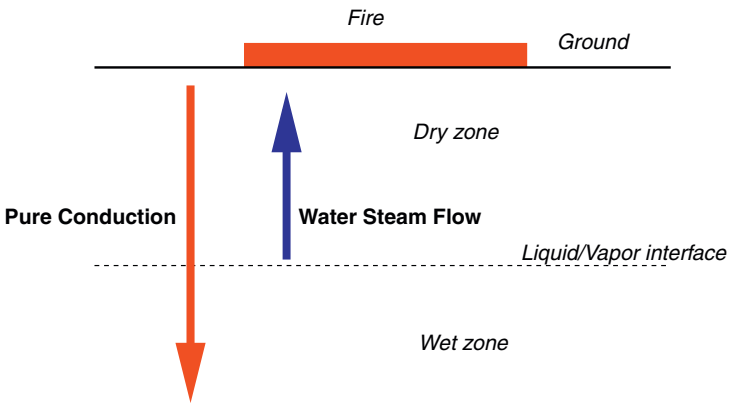

Figure 1. Physical description.

DOI: 10.1002/nme

where T_f and T_s are, respectively, the average of fluid and solid phase temperatures within a unit volume. V_f is the filtration velocity of Darcy for the fluid phase. The porosity ϕ, defined as the ratio of the volume of voids to the total volume, is assumed to be constant in both time and space. Additionally, λ_f is the effective thermal conductivity tensor for the fluid phase and h is the interfacial heat transfer coefficient per unit volume (Combarnous and Bories [15] describe h as the 'coefficient de transfert par unité de volume de milieu' and give units of $W/(cm^3{}^\circ C)$).

Likewise, the differential equation for the solid phase is given by

$$\operatorname{div}(\lambda_s \operatorname{grad} T_s) = \frac{\partial}{\partial t}[(1-\phi)(\rho C)_s T_s] + h(T_s - T_f) \tag{2}$$

In addition, λ_s is the effective thermal conductivity tensor for the solid phases. The overall effective thermal conductivity of the medium is given by

$$k_e = \lambda_f + \lambda_s \tag{3}$$

The effective thermal conductivity tensors λ_f and λ_s are used to incorporate the effects of hydrodynamic dispersion within the fluid phase and the dispersed structure of the porous medium. Neither the relationship between λ_f and k_f (thermal conductivity of the fluid phase) or λ_s and k_s (thermal conductivity of the porous matrix medium) is known *a priori*.

Subsequently, they assumed that the two phases are in local equilibrium, so that the energy conservation equation is expressed as

$$(\rho C)_e \frac{\partial T}{\partial t} + (\rho C)_f V_f \cdot \vec{\operatorname{grad}}\, T = \operatorname{div}(k_e \vec{\operatorname{grad}}\, T) \tag{4}$$

The effective calorific capacity being additive, the effective value $(\rho C)_e$ is then defined by the following equation:

$$\begin{aligned}(\rho C)_e &= \phi(\rho C)_f + (1-\phi)(\rho C)_s \\ &= \phi \rho_f C_f + (1-\phi)\rho_s C_s\end{aligned} \tag{5}$$

where ρ_s, C_s are constants, whereas ρ_f and C_f are temperature dependents.

On the other hand, when a heated region in the soil reaches T_v, the water presented in the soil turns into vapor flowing in the ground. To solve analytically or numerically the water steam flow problem (see Figure 1), we must first derive the differential equations. The obtention of differential equations requires the integration of conservation equations. First, in order to model the fluid motion through the porous medium, we use the Darcy flow model formulation presented by Wooding (1957)

$$V_f = -\frac{K}{\mu_f} \vec{\operatorname{grad}}\, P_f \tag{6}$$

where V_f is the filtration velocity of the fluid, K is the permeability (constant in time), μ_f is the viscosity of the fluid phase and P_f is the fluid pressure. Furthermore, the continuity equation is given by

$$\frac{\partial(\phi \rho_f)}{\partial t} + \operatorname{div}(\rho_f V_f) = 0 \tag{7}$$

The storage term can be clarified as follows if it is supposed that the porous environment is incompressible, i.e. if the porosity remains constant:

$$\frac{\partial(\phi \rho_f)}{\partial t} = \phi \frac{\partial \rho_f}{\partial t} + \rho_f \frac{\partial \phi}{\partial t} = \phi \frac{\partial \rho_f}{\partial t} \tag{8}$$

The resulting equation obtained by coupling (6), (8), which models the gas flowing in an isotropic medium, is thus given by

$$\operatorname{div}\left(\vec{\operatorname{grad}}\, P_f\right) = \frac{\phi \mu_f}{K \rho_f} \frac{\partial \rho_f}{\partial t} + \frac{1}{\mu_f} \vec{\operatorname{grad}}\, \mu_f \cdot \vec{\operatorname{grad}}\, P_f - \frac{1}{\rho_f} \vec{\operatorname{grad}}\, \rho_f \cdot \vec{\operatorname{grad}}\, P_f \tag{9}$$

DOI: 10.1002/nme

We assume that the water vapor obeys the ideal gas law

$$\frac{P_{\mathrm{f}}}{\rho_{\mathrm{f}} T_{\mathrm{f}}} = \beta = \text{ideal gas constant} \tag{10}$$

where T_{f} must be given in Kelvin.

Observing the phase transition problem for the fluid phase in which the evaporation takes place at a certain temperature T_{v}, two boundary conditions have to be specified, the first one for the edges of the computational domain which prescribes the geometrical form of the problem and the other one for the boundary between the dry and the wet zone. Let us define the two following regions: the first region with subscript 1 is saturated (porous matrix+liquid water); initially this humid region covers the entire domain of study, its temperature is constant and equals $T_1 = T_\infty$ and $\partial P_{\mathrm{f}}/\partial x = 0$. The second region, subscripted by 2, is a porous medium filled with water steam (we neglect the presence of air in the soil). For this dry region the boundary conditions at the surface $x = 0$ are: $T_C = T_{\mathrm{fire}}$ (temperature at the center of the fire) and $P_{\mathrm{f}} = P_{\mathrm{atm}}$ (atmospheric pressure).

Moreover, at the interface between the two regions, we have the continuity of the temperature

$$T_1 = T_2 = T_{\mathrm{v}} \quad \text{(temperature of evaporation)} \tag{11}$$

On the other hand, we have the discontinuity of the heat flux due to the phase change which writes

$$\left[\frac{1}{(\phi/k_{\mathrm{l}} + (1-\phi)/k_{\mathrm{s}})}\right]\frac{\partial T_1}{\partial x} - \left[\frac{1}{(\phi/k_{\mathrm{v}} + (1-\phi)/k_{\mathrm{s}})}\right]\frac{\partial T_2}{\partial x} = \phi L \frac{\partial \xi}{\partial t} \tag{12}$$

where L is the latent heat of the phase change per unit volume and ξ is the phase-change interface position. It should be noted that the combination achieved above uses a vertical configuration of components, which gives an harmonic average.

The mass flow of water steam created by the evaporation is proportional to the displacement of the interface $\partial\xi/\partial t$ of Equation (12). By the relation (6), we can transform this mass flow into pressure gradient, which becomes a Neumann boundary condition for P at the interface

$$\frac{\partial P_{\mathrm{f}}}{\partial x} = \frac{\mu_{\mathrm{f}}}{K}\frac{\rho_{\mathrm{l}}}{\rho_{\mathrm{v}}}\frac{\partial \xi}{\partial t} \tag{13}$$

3. AHC METHOD

To avoid the follow of the interface, the AHC method will be used. In this method, the latent heat is taken into account by integrating the heat capacity over the temperature [11], and the computational domain is considered as one region. As the relationship between heat capacity and temperature in isothermal problems involves sudden changes, the zero-width phase-change interval must be approximated by a narrow range of phase-change temperatures. The thermodynamic parameters of the fluid are defined considering the apparent capacity method of [11]. According to this reference, these parameters may be obtained taking into consideration that the phase change takes place in a small temperature interval (see Figure 2).

Then, if this interval is ΔT:

$$C_{\mathrm{f}} = \begin{cases} C_{\mathrm{l}}, & T < T_{\mathrm{v}} - \dfrac{\Delta T}{2} \\ \dfrac{C_{\mathrm{v}} + C_{\mathrm{l}}}{2} + \dfrac{\lambda}{\Delta T}, & T_{\mathrm{v}} - \dfrac{\Delta T}{2} \leqslant T \leqslant T_{\mathrm{v}} + \dfrac{\Delta T}{2} \\ C_{\mathrm{v}}, & T > T_{\mathrm{v}} + \dfrac{\Delta T}{2} \end{cases} \tag{14}$$

DOI: 10.1002/nme

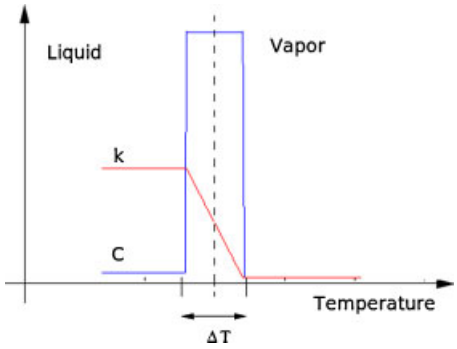

Figure 2. Physical properties given by Bonacina.

where $\lambda = L/\rho$. Similarly, a global new thermal conductivity has to be introduced:

$$k_{\mathrm{f}} = \begin{cases} k_l, & T < T_{\mathrm{v}} - \dfrac{\Delta T}{2} \\ k_{\mathrm{l}} + \dfrac{k_{\mathrm{v}} - k_{\mathrm{l}}}{\Delta T}\left[T - \left(T_{\mathrm{v}} - \dfrac{\Delta T}{2}\right)\right], & T v - \dfrac{\Delta T}{2} \leqslant T \leqslant T_{\mathrm{v}} + \dfrac{\Delta T}{2} \\ k_{\mathrm{v}}, & T > T_{\mathrm{v}} + \dfrac{\Delta T}{2} \end{cases} \tag{15}$$

The principal advantages of this approach are that (i) temperature T is the primary dependent variable that derives directly from the solution, and (ii) the use of this method usually reduces the fluctuations found by using the LHA approach [9]. As we mentioned above, the domain is considered as one region. A direct evaluation, in fact, can be expected to lead to satisfactory numerical integrations only if the thermophysical properties versus temperature curves do not present sharp peaks in the range of interest.

When the temperature approaches the phase-change temperature T_{v}, the equivalent heat capacity tends to the shape of Dirac δ function and, therefore, cannot be satisfactorily represented across the peak, by any smooth function. Such extreme problems can be successfully tackled by the technique proposed here, where a more appropriate averaging process is employed.

To overcome the abrupt change present in the formulations of thermophysical parameters defined by (14) and (15) (see Figure 2), we proposed to smooth these functions. The numerical solution can be obtained as the limit of a uniformly convergent sequence of classical solutions to approximating problems, deduced by smoothing the coefficients (14, 15), following a few general rules: the AHC formulation allows for a continuous treatment of a system involving phase transfer. If the phase transition takes place instantaneously at a fixed temperature, then a mathematical function such as

$$\sigma(T) = \chi(T - T_{\mathrm{v}}) \tag{16}$$

is representative of the volumetric fraction of the initial phase (liquid phase). χ is a step function whose value is zero when $T < T_{\mathrm{v}}$ and one otherwise. The variation of the initial phase fraction with temperature is

$$\frac{\mathrm{d}\sigma}{\mathrm{d}T} = \delta(T - T_{\mathrm{v}}) \tag{17}$$

in which $\delta(T - T_{\mathrm{v}})$ is the Dirac delta function whose value is infinity at the transition temperature, T_{v}, but zero at all other temperatures. To alleviate this singularity, the Dirac delta function can be approximated by the normal distribution function

$$\frac{\mathrm{d}\sigma}{\mathrm{d}T} = (\varepsilon\pi^{-1/2})\exp[-\varepsilon^2(T - T_{\mathrm{v}})^2] \tag{18}$$

DOI: 10.1002/nme

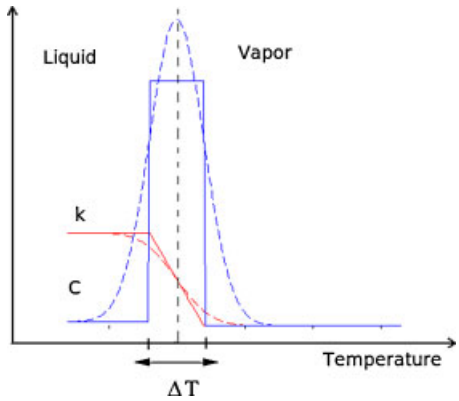

Figure 3. Smoothed physical properties.

in which ε is chosen to be $\varepsilon = 1/\sqrt{2}\Delta T$ and where ΔT is one-half of the assumed phase-change interval. Consequently, the integral of Equation (18) yields the error functions approximations for the initial phase fraction which is water in our case. With the conventional finite volume method, the initial phase fraction obtained from Equation (18) by integration should be used to avoid the numerical instabilities arising from the jump in the values of the volumetric fraction of initial phase from zero to one. The function σ is obtained by integrating $\mathrm{d}\sigma/\mathrm{d}T$ over temperature

$$\sigma(T) = \tfrac{1}{2}(1 + \operatorname{erf}(\varepsilon(T - T_{\mathrm{v}}))) \tag{19}$$

In our approach we assume for simplicity that the phases are isotropic and homogeneous. Accordingly, the smoothed coefficients (see Figure 3) of Equations (14) and (15) could be written as

$$C_{\mathrm{f}} = C_{\mathrm{l}} + (C_{\mathrm{v}} - C_{\mathrm{l}})\sigma(T) + L\frac{\mathrm{d}\sigma}{\mathrm{d}T} \tag{20}$$

and

$$k_{\mathrm{f}} = k_{\mathrm{l}} + (k_{\mathrm{v}} - k_{\mathrm{l}})\sigma(T) \tag{21}$$

To avoid the resolution of the problem in two different regions, the same approximations are used for all physical parameters: this is the key-point of our formulation. Indeed, a new formulation for the density is given by

$$\rho_{\mathrm{f}} = \rho_{\mathrm{l}} + (\rho_{\mathrm{v}} - \rho_{\mathrm{l}})\sigma(T) \tag{22}$$

where ρ_{l} remains constant and ρ_{v} is calculated using the ideal gas law (10), and Equation (22) could be written as follows:

$$\rho_{\mathrm{f}} = \rho_{\mathrm{l}} + \left(\frac{P}{\beta T} - \rho_{\mathrm{l}}\right)\sigma(T) \tag{23}$$

Also, a new formulation for the viscosity is given by

$$\mu_{\mathrm{f}} = \mu_{\mathrm{l}} + (\mu_{\mathrm{v}} - \mu_{\mathrm{l}})\sigma(T) \tag{24}$$

where

$$\mu_{\mathrm{l}} = 0.4527(T + 40)^{-1.492}$$

and

$$\mu_{\mathrm{v}} = 122.10^{-7} + 4.10^{-8}(T - T_{\mathrm{v}})$$

T is given in Celsius degree. These linear approximations of the liquid water and vapor viscosities are obtained from the Fortran 90 library NBS steam tables (`http://people.scs.fsu.edu/~burkardt/f_src/steam/steam.html`) that computes various physical properties of water, related to temperature and pressure.

DOI: 10.1002/nme

4. SET OF EQUATIONS

Using the new formulations of physical parameters as given in the previous section, the system of coupled equations to be solved is written as follows:

$$(\rho C)_{\mathrm{e}}(T)\frac{\partial T(x,t)}{\partial t}-\frac{K(\rho C)_{\mathrm{f}}(T)}{\mu_{\mathrm{f}}(T)}\vec{\mathrm{grad}}\,P(x,t)\cdot\vec{\mathrm{grad}}\,T(x,t)$$

$$-\mathrm{div}[k_{\mathrm{e}}\vec{\mathrm{grad}}\,T(x,t)]=0 \quad \text{in } \Omega\times(0,t_{\mathrm{end}}]$$

$$\frac{\sigma(T)}{T(x,t)\beta}\frac{\partial P(x,t)}{\partial t}+\left[\left(\frac{P(x,t)}{T(x,t)\beta}-\rho_{\mathrm{l}}\right)\frac{\mathrm{d}\sigma(T)}{\mathrm{d}T}-\frac{P(x,t)}{T^2(x,t)\beta}\sigma(T)\right]\frac{\partial T(x,t)}{\partial t}$$

$$+\frac{K\rho_{\mathrm{f}}(T)}{\phi\mu_{\mathrm{f}}(T)}\left(\frac{1}{\mu_{\mathrm{f}}(T)}\vec{\mathrm{grad}}\,\mu_{\mathrm{f}}(T)-\frac{1}{\rho_{\mathrm{f}}(T)}\vec{\mathrm{grad}}\,\rho_{\mathrm{f}}(T)\right)\vec{\mathrm{grad}}\,P(x,t)$$

$$-\frac{K\rho_{\mathrm{f}}(T)}{\phi\mu_{\mathrm{f}}(T)}\mathrm{div}(\vec{\mathrm{grad}}\,P(x,t))=0 \quad \text{in } \Omega\times(0,t_{\mathrm{end}}]$$

$$\begin{aligned}
T(x,0)&=T_0(x) && \text{in } \Omega\\
T(x,t)&=T^{\mathrm{D}}(x,t) && \text{on } \Gamma^{\mathrm{D}}\times(0,t_{\mathrm{end}}]\\
\nabla T(x,t).v&=q^{\mathrm{N}}(x,t) && \text{on } \Gamma^{\mathrm{N}}\times(0,t_{\mathrm{end}}]\\
P(x,0)&=P_0(x) && \text{in } \Omega\\
P(x,t)&=P^{\mathrm{D}}(x,t) && \text{on } \Gamma^{\mathrm{D}}\times(0,t_{\mathrm{end}}]\\
\nabla P(x,t).v&=s^{\mathrm{N}}(x,t) && \text{on } \Gamma^{\mathrm{N}}\times(0,t_{\mathrm{end}}]
\end{aligned} \tag{25}$$

where Ω is a bounded domain in $\mathbb{R}^d$ $(d=1,\ldots,3)$ with boundary $\partial\Omega=\Gamma^{\mathrm{D}}\cup\Gamma^{\mathrm{N}}$; T represents the temperature, P is the pressure variable; ρ is the density, C is the AHC, μ is the viscosity, ϕ is the porosity, the subscripts e, f and s indicate, respectively, the equivalent parameters of the medium, the properties of the fluid and the porous matrix properties; k_{e} is the conductivity, it is assumed to be a diagonal tensor with components in $L^{\infty}(\Omega)$ (k_{e} is calculated using the harmonic mean between k_{f} and k_{s}); K is the permeability; v indicates the outward unit normal vector along $\partial\Omega$; T^{D} and q^{N} are, respectively, the Dirichlet and Neumann boundary conditions for the temperature; P^{D} and s^{N} are, respectively, the Dirichlet and Neumann boundary conditions for the pressure. It should be emphasized that the thermophysical properties of the fluid are temperature dependent and the problem is non-linear.

However, with adequate initial and boundary conditions, the problem to be solved (25) may be written in the vectorial form

$$\begin{aligned}
\frac{\partial T}{\partial t}&=f(t,x,T,P)\\
\gamma\frac{\partial T}{\partial t}+\theta\frac{\partial P}{\partial t}&=g(t,x,T,P)
\end{aligned} \tag{26}$$

where γ and θ are two variables dependent on $\sigma(T)$ (19) and $\mathrm{d}\sigma/\mathrm{d}T$ (18).

5. NUMERICAL METHODS

The first equation of the system (26) is an ordinary differential one. On the other hand, the second equation is a differential algebraic one because $\sigma(T)=0$ and/or $\mathrm{d}\sigma/\mathrm{d}T=0$ for $T<T_{\mathrm{v}}$; hence, we

DOI: 10.1002/nme

have a DAE. The numerical resolution of non-linear systems with partial differential algebraic equations (PDAE) is very complicated. Concerning the heat diffusion and the water steam flow in saturated porous media, systems could have very large size and present high non-linearity. These systems are difficult to solve in spite of the great diversity of existing possible approaches, because extension to DAE systems stresses the numerical method. For this reason, there is a lack of methods that could deal with all types of systems of PDAE.

Among the large variety of existing approaches used to solve PDAE systems, we choose the following methodology:

1. The use of the method of lines, where space and time discretizations are considered separately.
2. Spatial discretization: finite volume method because it conserves mass locally and preserves the continuity of fluxes.
3. Time discretization: The Euler implicit scheme.
4. The use of a modified Newton method to deal with the present non-linearity.

However, various criteria are concerned by defining the reliable method:

- the precision of the results,
- the stability of the method,
- the computational cost,
- the facility of implementation.

In addition, a combination between all these criteria must take into account all the presented difficulties (advection–diffusion heat transfer, phase change, interface tracking, coupling with water steam flow, stiff system, high non-linearity, etc.)

Using the method of lines, the system of equations is discretized (25) basing on the finite volume method. The diffusion–dispersion terms are discretized implicitly in time with a vertex-centered finite volume discretization in space; hence, the size of time step is limited only by the desired precision. Otherwise, with an implicit scheme, each time step leads to a global non-linear system of equations, where heat diffusion with phase change and water steam flow are coupled. Therefore, it is necessary to solve non-linear coupled equations.

On the other hand, for the convection–advection term in the energy equation of the system (25), an upwind finite volume scheme in space and an explicit scheme in time [16] are used. The upstream choice allows us to deal with all sizes of velocities. The explicit time discretization choice requires the respect of CFL condition, but it has the advantage that it conserves the symmetry of the linear system to be solved at each time step. However, the criterion on the choice of the time step due to the explicit scheme for the advection term obliges us to use a small time step in comparison with the required one for the diffusion–dispersion terms.

In our case, the proposed scheme as described above is computationally expensive; hence, we use an implicit backward differentiation formula (BDF) method (as in [17]) that adapts the time step in such a way so as to find the desired precision and to avoid instabilities.

6. SPATIAL DISCRETIZATION USING FINITE-VOLUME METHOD

The set of equations presented above are cast in the usual finite volume form for a finite domain: each cell (or control volume) encloses exactly one data node at x_i and its boundaries are always computed as the middle of two consecutive nodes; hence, we obtain a good accuracy in the gradient estimation. We denote by T_i the whole approximate solution of temperature and by P_i the approximate solution of pressure, the location of any variables being indicated by subscripts.

To apply the finite-volume method, we first divide the problem domain into a finite-volume grid or mesh (i.e. series of cells or blocks), in this case of equal width, Δx, as shown in Figure 4.

For instance, the temperature at face $i+\frac{1}{2}$ is $T_{i+1/2}=T_i f_{i+1/2}+T_{i+1}(1-f_{i+1/2})$ where $f_{i+1/2}=(2\delta x_{i+1/2}-\Delta x_i)/2\delta x_{i+1/2}$, $\Delta x_i=x_{i+1/2}-x_{i-1/2}$, $\delta x_{i+1/2}=x_{i+1}-x_i$, and $\delta x_{i-1/2}=x_i-x_{i-1}$. A uniform mesh is used; hence $\Delta x_i=\Delta x \forall i$. The other variable that has to be approximated at

DOI: 10.1002/nme

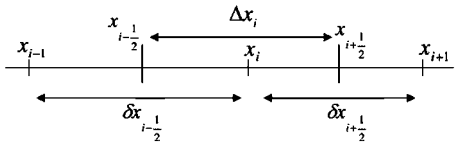

Figure 4. Block-centered finite-volume discretization of a one-dimensional problem domain.

cell faces is the interface conductivity; the harmonic mean is used for composite materials for its superior handling of abrupt property changes by recognizing that the primary interest is to obtain a good representation of heat flux across interfaces rather than that of the conductivity [9] (Patankar, 1980):

$$\frac{1}{k_{\mathrm{e}}}=\frac{1-f_{i+1/2}}{k_i}+\frac{f_{i+1/2}}{k_{i+1}} \tag{27}$$

6.1. Spatial discretization of (25) *for the 1D case*

At each time step, the 1D energy equation is numerically integrated over the control volume by taking Figure 4 as reference:

$$\int_{x_{i-1/2}}^{x_{i+1/2}}(\rho C)_{\mathrm{e}}\frac{\partial T}{\partial t}\,\mathrm{d}x+\int_{x_{i-1/2}}^{x_{i+1/2}}(\rho C)_{\mathrm{f}}V_{\mathrm{f}}\frac{\partial T}{\partial x}\,\mathrm{d}x=\int_{x_{i-1/2}}^{x_{i+1/2}}\frac{\partial}{\partial x}\left(k_{\mathrm{e}}\frac{\partial T}{\partial x}\right)\mathrm{d}x,\quad 2\leqslant i\leqslant N-1 \tag{28}$$

For the transient term, it is assumed that the temperature of the control volume is represented by that of the node:

$$\int_{x_{i-1/2}}^{x_{i+1/2}}(\rho C)_{\mathrm{e}}\frac{\partial T}{\partial t}\,\mathrm{d}x=(\rho C)_{\mathrm{e},i}\,\frac{\mathrm{d}T_i}{\mathrm{d}t}\Delta x=(\rho C)_{\mathrm{e}}(T_i)\,\frac{\mathrm{d}T_i}{\mathrm{d}t}\Delta x,\quad 2\leqslant i\leqslant N-1 \tag{29}$$

The diffusion term is approximated by using the piecewise-linear temperature profile. For instance:

$$\int_{x_{i-1/2}}^{x_{i+1/2}}k_{\mathrm{e}}\frac{\partial^2 T}{\partial x^2}\,\mathrm{d}x=\left[k_{\mathrm{e}}|_{i+1/2}\frac{T_{i+1}-T_i}{\Delta x}-k_{\mathrm{e}}|_{i-1/2}\frac{T_i-T_{i-1}}{\Delta x}\right],\quad 2\leqslant i\leqslant N-1 \tag{30}$$

For the convection term, the central weighting scheme tends to create artificial oscillation. Specifically, the numerical solution oscillates around the true solution. Because of these problems, alternative spatial weighting schemes have been developed. A frequently used scheme is the upstream (also called upwind) scheme ([18, 19]), which can be expressed as follows:

$$T_{i+1/2}=(1-\alpha)T_i+\alpha T_{i+1},\quad 2\leqslant i\leqslant N-1$$

where

$$\alpha=\begin{cases}0 & \text{if } V>0\\ 1 & \text{if } V<0\end{cases}$$

We replace V_{f} by its value by using (6); hence, we obtain

$$\begin{aligned}\int_{x_{i-1/2}}^{x_{i+1/2}}(\rho C)_f V_{\mathrm{f}}\frac{\partial T}{\partial x}\,\mathrm{d}x&=-\int_{x_{i-1/2}}^{x_{i+1/2}}\frac{K(\rho C)_{\mathrm{f}}}{\mu_{\mathrm{f}}}\frac{\partial P}{\partial x}\frac{\partial T}{\partial x}\,\mathrm{d}x\\&=-\frac{K(\rho C)_{f,i}}{\mu_{f,i}\Delta x}(T_{i+1/2}-T_{i-1/2})(P_{i+1}-P_{i-1}),\quad 2\leqslant i\leqslant N-1\end{aligned} \tag{31}$$

DOI: 10.1002/nme

By substituting the approximated terms in (29), (30), (31) into (28) for a uniform mesh, the discretized equation for a control volume is obtained as

$$\frac{\mathrm{d}T_i}{\mathrm{d}t}-\frac{K(\rho C)_{f,i}}{2\mu_{f,i}(\rho C)_{\mathrm{e},i}\Delta x^2}[(1-\alpha)(T_i-T_{i-1})+\alpha(T_{i+1}-T_i)](P_{i+1}-P_{i-1})$$
$$-\frac{k_{i+1}+k_i}{2(\rho C)_{\mathrm{e},i}\Delta x^2}(T_{i+1}-T_i)-\frac{k_i+k_{i-1}}{2(\rho C)_{\mathrm{e},i}\Delta x^2}(T_i-T_{i-1})=0, 2\leqslant i\leqslant N-1 \tag{32}$$

To discretize the equation of water steam flow in the system (25), we use the integration by parts; the discretization is given by the following formulation:

$$\frac{\sigma(T_i)}{T_i\beta}\frac{\mathrm{d}P_i}{\mathrm{d}t}+\left[\left(\frac{P_i}{T_i\beta}-\rho_{\mathrm{l}}\right)\frac{\mathrm{d}\sigma(T_i)}{\mathrm{d}T_i}-\frac{P_i}{T_i^2\beta}\sigma(T_i)\right]\frac{\mathrm{d}T_i}{\mathrm{d}t}$$
$$+\frac{K\rho_{f,i}}{\phi\mu_{f,i}\Delta x^2}\left[\log\left(\frac{\mu_{f,i+1}+\mu_{f,i}}{\rho_{f,i+1}+\rho_{f,i}}\right)-\log\left(\frac{\mu_{f,i}}{\rho_{f,i}}\right)-1\right]P_{i+1}$$
$$-\frac{K\rho_{f,i}}{\phi\mu_{f,i}\Delta x^2}\left[\log\left(\frac{\mu_{f,i+1}+\mu_{f,i}}{\rho_{f,i+1}+\rho_{f,i}}\right)+\log\left(\frac{\mu_{f,i}+\mu_{f,i-1}}{\rho_{f,i}+\rho_{f,i-1}}\right)-2\log\left(\frac{\mu_{f,i}}{\rho_{f,i}}\right)-2\right]P_i$$
$$+\frac{K\rho_{f,i}}{\phi\mu_{f,i}\Delta x^2}\left[\log\left(\frac{\mu_{f,i}+\mu_{f,i-1}}{\rho_{f,i}+\rho_{f,i-1}}\right)-\log\left(\frac{\mu_{f,i}}{\rho_{f,i}}\right)-1\right]P_{i-1}=0,\quad 2\leqslant i\leqslant N-1 \tag{33}$$

The initial and boundary conditions are written as follows:

$$\begin{aligned}
&T(x_i,0)=T_0(x_i)=T_{0,i}, && 1\leqslant i\leqslant N\\
&T(x_i,t)=T^{\mathrm{D}}(x_i,t)=T_i^{\mathrm{D}}(t), && i=1 \quad \text{or} \quad i=N\\
&\nabla T(x_i,t).v=q^{\mathrm{N}}(x_i,t)=q_i^{\mathrm{N}}(t), && i=1 \quad \text{or} \quad i=N\\
&P(x_i,0)=P_0(x_i)=P_{0,i}, && 1\leqslant i\leqslant N\\
&P(x_i,t)=P^{\mathrm{D}}(x_i,t)=P_i^{\mathrm{D}}(t), && i=1 \quad \text{or} \quad i=N\\
&\nabla P(x_i,t).v=s^{\mathrm{N}}(x_i,t)=s_i^{\mathrm{N}}(t), && i=1 \quad \text{or} \quad i=N
\end{aligned} \tag{34}$$

6.2. Spatial discretization for 3D axisymmetric problem

The 3D axisymmetric solution is based on the 3D Fourier's equation expressed in cylindrical coordinates in which it is assumed to be no dependence on the azimuthal coordinate. Then, the axisymmetric energy equation can be written as follows:

$$(\rho C)_{\mathrm{e}}\frac{\partial T}{\partial t}+(\rho C)_{\mathrm{f}}\left[V_r\frac{\partial T}{\partial r}+V_z\frac{\partial T}{\partial z}\right]=\frac{1}{r}\frac{\partial}{\partial r}\left(kr\frac{\partial T}{\partial r}\right)+\frac{\partial}{\partial z}\left(k\frac{\partial T}{\partial z}\right) \tag{35}$$

The water steam flow equation is written with the cylindrical coordinates as follows:

$$\frac{\sigma(T)}{\beta T}\frac{\partial P}{\partial t}+\left[\left(\frac{P}{T\beta}-\rho_{\mathrm{l}}\right)\frac{\mathrm{d}\sigma(T)}{\mathrm{d}T}-\frac{P}{T^2\beta}\sigma(T)\right]\frac{\partial T}{\partial t}$$
$$+\frac{K\rho_{\mathrm{f}}}{\phi\mu_{\mathrm{f}}}\left(\frac{1}{\mu_{\mathrm{f}}}\frac{\partial\mu_{\mathrm{f}}}{\partial r}-\frac{1}{\rho_{\mathrm{f}}}\frac{\partial\rho_{\mathrm{f}}}{\partial r}\right)\frac{\partial P}{\partial r}+\frac{K\rho_{\mathrm{f}}}{\phi\mu_{\mathrm{f}}}\left(\frac{1}{\mu_{\mathrm{f}}}\frac{\partial\mu_{\mathrm{f}}}{\partial z}-\frac{1}{\rho_{\mathrm{f}}}\frac{\partial\rho_{\mathrm{f}}}{\partial z}\right)\frac{\partial P}{\partial z}$$
$$-\frac{K\rho_{\mathrm{f}}}{\phi\mu_{\mathrm{f}}r}\frac{\partial}{\partial r}\left(r\frac{\partial P}{\partial r}\right)-\frac{K\rho_{\mathrm{f}}}{\phi\mu_{\mathrm{f}}}\frac{\partial^2 P}{\partial z^2}=0 \tag{36}$$

where all terms are as previously defined.

DOI: 10.1002/nme

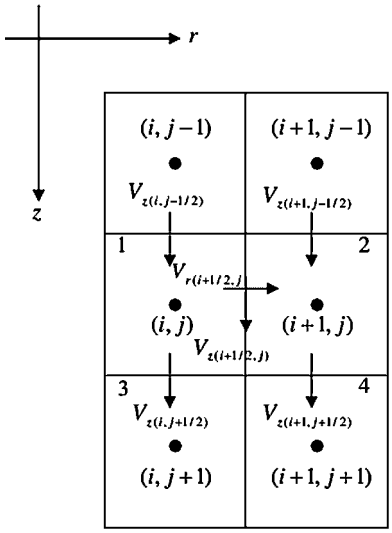

Figure 5. Evaluation of the interface velocity components. At the interface between nodes (i, j) and $(i, j+1)$, $V_{r(i,j+1/2)}$ is directly known from the flow model. In contrast, $V_{z(i,j+1/2)}$ must be interpolated from values at interfaces labeled 1, 2, 3 and 4.

The spatial discretization is performed by integrating the system of equations over the cells. In fact, in this section we present the discretization of the convection–advection terms using an upwind scheme (see Figure 5). The net advective flux into cell (i, j) in the r direction can be approximated by the finite-volume method as

$$\int_{i-1/2}^{i+1/2}\int_{j-1/2}^{j+1/2} V_r \frac{\partial T}{\partial r} r\,\mathrm{d}r\,\mathrm{d}z = r_i[V_{r(i+1/2,j)}((1-\alpha_1)T_{i,j}+\alpha_1 T_{i+1,j}) - V_{r(i-1/2,j)}((1-\alpha_1)T_{i-1,j}+\alpha_1 T_{i,j})]\Delta z \tag{37}$$

where $2\leqslant i\leqslant N-1$ and $2\leqslant j\leqslant M-1$.

The net advective flux into cell (i, j) in the z direction can be approximated by the finite-volume method as

$$\int_{i-1/2}^{i+1/2}\int_{j-1/2}^{j+1/2} V_z \frac{\partial T}{\partial z} r\,\mathrm{d}r\,\mathrm{d}z = \frac{r_{i+1}^2+2r_i(r_{i+1}-r_{i-1})-r_{i-1}^2}{8} \times[V_{z(i,j+1/2)}((1-\alpha_2)T_{i,j}+\alpha_2 T_{i,j+1}) - V_{z(i,j-1/2)}((1-\alpha_2)T_{i,j-1}+\alpha_2 T_{i,j})] \tag{38}$$

where $2\leqslant i\leqslant N-1$ and $2\leqslant j\leqslant M-1$.

The spatial weighting factors, α_1 and α_2, are equal to 0.5 for the central scheme, and 0 or 1 for the upstream scheme depending on the direction of the flow vectors at the cell interfaces [18, 19].

The energy equation is discretized by using the upwind scheme for the convection–advection terms and the vertex-centered scheme for the diffusion–dispersion terms:

$$\frac{\mathrm{d}T_{i,j}}{\mathrm{d}t} - \frac{2(k_{i+1,j}+k_{i,j})(r_{i+1}+r_i)}{(\rho C)_{\mathrm{e},i,j}[r_{i+1}^2+2r_i(r_{i+1}-r_{i-1})-r_{i-1}^2]\Delta r}(T_{i+1,j}-T_{i,j}) + \frac{2(k_{i,j}+k_{i-1,j})(r_i+r_{i-1})}{(\rho C)_{\mathrm{e},i,j}[r_{i+1}^2+2r_i(r_{i+1}-r_{i-1})-r_{i-1}^2]\Delta r}(T_{i,j}-T_{i-1,j})$$

DOI: 10.1002/nme

$$
\begin{aligned}
&-\frac{k_{i,j+1}+k_{i,j}}{2(\rho C)_{\mathrm{e},i,j}\Delta z^2}(T_{i,j+1}-T_{i,j})+\frac{k_{i,j}+k_{i,j-1}}{2(\rho C)_{\mathrm{e},i,j}\Delta z^2}(T_{i,j}-T_{i,j-1})\\
&+\frac{8(\rho C)_{f,i,j}r_i}{(\rho C)_{\mathrm{e},i,j}[r_{i+1}^2+2r_i(r_{i+1}-r_{i-1})-r_{i-1}^2]}[V_{r(i+1/2,j)}((1-\alpha_1)T_{i,j}+\alpha_1 T_{i+1,j})\\
&-V_{r(i-1/2,j)}((1-\alpha_1)T_{i-1,j}+\alpha_1 T_{i,j})]\\
&+\frac{(\rho C)_{f,i,j}}{(\rho C)_{\mathrm{e},i,j}\Delta z}[V_{z(j+1/2,j)}((1-\alpha_2)T_{i,j}+\alpha_2 T_{i,j+1})-V_{z(j-1/2,j)}((1-\alpha_2)T_{i,j-1}+\alpha_2 T_{i,j})]=0
\end{aligned}
\tag{39}
$$

where $2\leqslant i\leqslant N-1$ and $2\leqslant j\leqslant M-1$.

The water steam flow equation is also discretized and it could be written as follows:

$$
\begin{aligned}
&\frac{\sigma(T_{i,j})}{\beta T_{i,j}}\frac{\mathrm{d}P_{i,j}}{\mathrm{d}t}+\left[\left(\frac{P_{i,j}}{T_{i,j}\beta}-\rho_{\mathrm{l}}\right)\frac{\mathrm{d}\sigma(T_{i,j})}{\mathrm{d}T}-\frac{P_{i,j}}{T_{i,j}^2\beta}\sigma(T_{i,j})\right]\frac{\mathrm{d}T_{i,j}}{\mathrm{d}t}\\
&+\frac{K\rho_{f_{i,j}}}{\phi\mu_{f_{i,j}}}\frac{8}{(r_{i+1}^2+2r_ir_{i+1}-3r_i^2)\Delta r}\left[r_i\log\left(\frac{\mu_{f_{i+1,j}}+\mu_{f_{i,j}}}{\rho_{f_{i+1,j}}+\rho_{f_{i,j}}}\right)-r_i\log\left(\frac{\mu_{f_{i,j}}}{\rho_{f_{i,j}}}\right)-\frac{r_{i+1}-r_i}{2}\right]P_{i+1,j}\\
&+\frac{K\rho_{f_{i,j}}}{\phi\mu_{f_{i,j}}\Delta z^2}\left[\log\left(\frac{\mu_{f_{i,j+1}}+\mu_{f_{i,j}}}{\rho_{f_{i,j+1}}+\rho_{f_{i,j}}}\right)-\log\left(\frac{\mu_{f_{i,j}}}{\rho_{f_{i,j}}}\right)-1\right]P_{i,j+1}\\
&+\frac{K\rho_{f_{i,j}}}{\phi\mu_{f_{i,j}}\Delta z^2}\left[\log\left(\frac{\mu_{f_{i,j-1}}+\mu_{f_{i,j}}}{\rho_{f_{i,j-1}}+\rho_{f_{i,j}}}\right)-\log\left(\frac{\mu_{f_{i,j}}}{\rho_{f_{i,j}}}\right)-1\right]P_{i,j-1}\\
&-\frac{K\rho_{f_{i,j}}}{\phi\mu_{f_{i,j}}}\frac{8}{(r_{i+1}^2+2r_ir_{i+1}-3r_i^2)\Delta r}\left[r_i\log\left(\frac{\mu_{f_{i+1,j}}+\mu_{f_{i,j}}}{\rho_{f_{i+1,j}}+\rho_{f_{i,j}}}\right)-r_i\log\left(\frac{\mu_{f_{i,j}}}{\rho_{f_{i,j}}}\right)-\frac{r_{i+1}-r_i}{2}\right]P_{i,j}\\
&-\frac{K\rho_{f_{i,j}}}{\phi\mu_{f_{i,j}}\Delta z^2}\left[\log\left(\frac{\mu_{f_{i,j+1}}+\mu_{f_{i,j}}}{\rho_{f_{i,j+1}}++\rho_{f_{i,j}}}\right)\log\left(\frac{\mu_{f_{i,j-1}}+\mu_{f_{i,j}}}{\rho_{f_{i,j-1}}+\rho_{f_{i,j}}}\right)-2\log\left(\frac{\mu_{f_{i,j}}}{\rho_{f_{i,j}}}\right)-2\right]P_{i,j}=0
\end{aligned}
\tag{40}
$$

where $2\leqslant i\leqslant N-1$ and $2\leqslant j\leqslant M-1$.

The discretized initial and boundary conditions are given by:

$$
\begin{aligned}
T(r_i,z_j,0)&=T_0(r_i,z_j)=T_{0,i,j},\quad 1\leqslant i\leqslant N,\ \ 1\leqslant j\leqslant M\\
T(r_i,z_j,t)&=T^{\mathrm{D}}(r_i,z_j,t)=T_{i,j}^{\mathrm{D}}(t),\quad i\in\{1,N\}\text{ and }j\in\{1,M\}\\
\nabla T(r_i,z_j,t).v&=q^{\mathrm{N}}(r_i,z_j,t)=q_{i,j}^{\mathrm{N}}(t),\quad i\in\{1,N\}\text{ and }j\in\{1,M\}\\
P(r_i,z_j,0)&=P_0(r_i,z_j)=P_{0,i,j},\quad 1\leqslant i\leqslant N,\ \ 1\leqslant j\leqslant M\\
P(r_i,z_j,t)&=P^{\mathrm{D}}(r_i,z_j,t)=P_{i,j}^{\mathrm{D}}(t),\quad i\in\{1,N\}\text{ and }j\in\{1,M\},\\
\nabla P(r_i,z_j,t)\cdot v&=s^{\mathrm{N}}(r_i,z_j,t)=s_{i,j}^{\mathrm{N}}(t),\quad i\in\{1,N\}\text{ and }j\in\{1,M\},
\end{aligned}
\tag{41}
$$

6.3. The derived algebraic system

By using the method of lines, functions T and P are transformed into $2N$ vectors corresponding to their values at each discretization point. The spatial derivatives are approximated using finite-volume formula on three points where the best results for accuracy and computation time efficiency were obtained.

DOI: 10.1002/nme

The spatial discretization of the energy equation presented above (39) is written under the form

$$S(T)\frac{\mathrm{d}T}{\mathrm{d}t}+A(T)T+B(T,P)T=b \tag{42}$$

where $S(T)$ is a non-singular diagonal matrix such as $S(T)_i=(\rho C)_e(T_i)\neq 0\forall i\in[1,N]$. The coefficients of the matrices $A(T)$ and $B(T,P)$ are obtained by the spatial discretization of the energy equation (39). b is the second member vector. Equation (42) is an ordinary differential equation that writes:

$$\frac{\mathrm{d}T}{\mathrm{d}t}+S(T)^{-1}A(T)T+S(T)^{-1}B(T,P)T=S(T)^{-1}b \tag{43}$$

Also, the water steam flow equation writes after the spatial discretization:

$$D(T,P)\frac{\mathrm{d}T}{\mathrm{d}t}+C(T)\frac{\mathrm{d}P}{\mathrm{d}t}+E(T)P=c \tag{44}$$

where $D(T,P)$ and $C(T)$ are two diagonal matrices and $C(T)$ is singular because $C(T)_i=0$ when $\sigma(T_i)=0$, for V_i control volume; the equation is then an algebraic one. The coefficients of the matrix $E(T)$ are obtained by the discretization of the flow problem (40) and c is the second member vector.

Combining (43) and (44), we obtain the following algebraic system:

$$\begin{pmatrix} I & 0 \\ D(T,P) & C(T) \end{pmatrix}\begin{pmatrix} \dfrac{\mathrm{d}T}{\mathrm{d}t} \\ \dfrac{\mathrm{d}P}{\mathrm{d}t} \end{pmatrix}+\begin{pmatrix} S(T)^{-1}(A(T)+B(T,P)) & 0 \\ 0 & E(T) \end{pmatrix}\begin{pmatrix} T \\ P \end{pmatrix}=\begin{pmatrix} S(T)^{-1}b \\ c \end{pmatrix} \tag{45}$$

Let $Y=[T,P]^T$. By classical transformations, the system can be written in the general form

$$M\frac{\mathrm{d}Y}{\mathrm{d}t}+f(Y)=0 \tag{46}$$

where

$$M=\begin{pmatrix} I & 0 \\ D(T,P) & C(T) \end{pmatrix},\quad f(Y)=\begin{pmatrix} S(T)^{-1}(A(T)+B(T,P))T-S(T)^{-1}b \\ E(T)P-c \end{pmatrix}$$

We denote by J the jacobian matrix of f.

7. RESOLUTION OF THE DAE SYSTEM USING AN APPROPRIATE SOLVER

We start by considering the semi-discrete diffusion–convection model as a system of DAE of index one and then we use the framework of DAE solvers. Indeed, it is sufficient to differentiate the algebraic flow equations in order to get a system of ODE. Thus, the differentiation index of the system is equal to one here.

In classical global approaches, an implicit Euler scheme is used to solve (46). This leads, at each time step, to the non-linear system $MY+\Delta t f(Y)-MY_n=0$ and the Jacobian of this system is the matrix $M+\Delta t J$. This system can be solved by a Newton method. Newton iterations are written as follows:

$$(M+\Delta t J)(Y^{k+1}-Y^k)=-(MY^k+\Delta t f(Y^k)-MY_n) \tag{47}$$

7.1. Our global approach

We claim that an efficient way to solve our problem is to use a specific DAE solver with an implicit time discretization. Our approach is a generalization of the classical global approach, which is a

DOI: 10.1002/nme

particular case with an implicit Euler scheme and a fixed time step. Thus, we keep the advantage of the robustness of the method and compared with the fixed implicit scheme as Euler used in the classical global approach; a big advantage of DAE solvers is their control of accuracy with a variable order scheme. Moreover, these solvers provide a control of time step and the associated control of Jacobian updates (ensuring convergence of Newton iterations for example). It is in principle possible to implement these controls, but they are rather sophisticated in DAE solvers and not so easy to reproduce.

In order to solve the DAE system (46), we adopt the following strategy. We use software libraries and write modules clearly identified as diffusion and flow. We apply a DAE solver (in our experiments, the `DASSL` DAE solver of `SLATEC`, to which we provide the temperature-dependent mass matrix M, the function f, the Jacobian J and consistent initial conditions). We start by calculating $Y_0^{'}$ from Y_0 using a routine that we implemented in the DAE solver following the algorithm used by `MATLAB` [20] to calculate the initial conditions at the time $t = t_0$. Then the DAE solver applies a time discretization scheme using the BDF method and solves at each time step a system of non-linear equations using a modified Newton method [21, 22].

A drawback of our approach is the large size of the linear system; however, the matrix is sparse. Thus, to improve efficiency we use a sparse linear solver (`UMFPACK` library) in the algorithm of Newton-LU in `DASSL`.

The whole software uses the Fortran 90 `MUESLI` library (`http://www.irisa.fr/sage/edouard/canot/muesli/`), which provides linear algebra facilities using a `Matlab`-like syntax.

8. DEVELOPED SOFTWARE

Two programs have been developed using the numerical strategy presented above, both are developed in one, two and 3D-axisymmetric cases: the first one `DIFFUSE-WC` allows to simulate the heat transfer in saturated porous media by neglecting the convective effect (phase change `W`ithout `C`oupling with vapor flow); the second one is `DIFFUSE-C` that simulates the heat transfer in saturated porous media taking into account the `C`oupling effect between the heat transfer with phase change and the vapor flow in the ground.

9. NUMERICAL EXPERIMENTS

9.1. Performance and cost

In order to obtain good performances in our global approach, the Jacobian matrix is calculated explicitly and coded by hand. Actually, we modified the DAE solver `DASSL` in such a way that it could support sparse jacobian matrix using the compact sparse column format (CSC) respecting the `UMFPACK` library requirement. The advantages of sparse matrices are both size and speed. For example, a 100×100 matrix needs about 110 MB for dense storage and leads to 38 h for its resolutions using a 2.1 GHz Dual Core-2 machine. On the other hand, the storage size falls to 15 MB (38 342 non-zero elements) and the CPU time falls to 87 s on the same machine. The speed advantage of sparse matrix is illustrated in Figure 6.

9.2. Effect of the coupling with water steam flow

In order to show the effect of coupling between the heat transfer with phase change and the water steam flow in the ground, we simulate the heat diffusion in a water saturated soil and we compare the results in both cases (with and without coupling). We consider a water saturated clay soil initially at 20°C, the temperature of the supposed fire at the surface of the soil is 300°C. The curves illustrated in Figure 7 represent the temperature histories at 5 and 2.5 cm depths in the soil for both cases (with and without coupling with water steam flow). Indeed, this figure shows the retarding effect of steam convection; this is due to the fact that the vapor flowing in the ground

DOI: 10.1002/nme

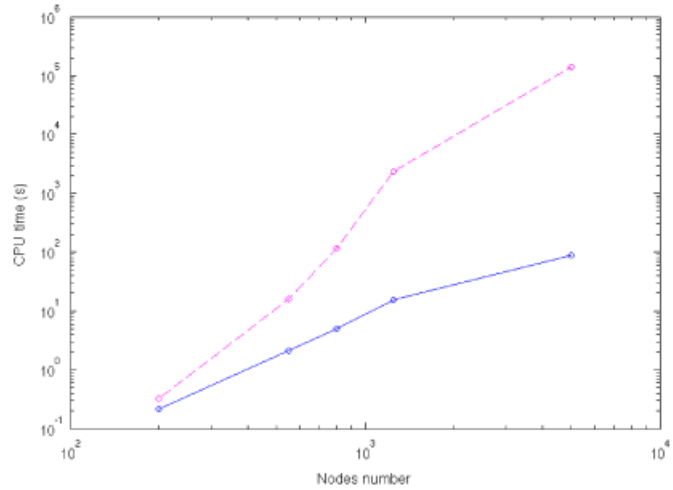

Figure 6. CPU time versus the nodes number used in the simulation with sparse matrix (solid curve) and dense matrix (dashed curve) structures. Used grids are: 10×10, 15×15, 20×20, 25×25 and 50×50.

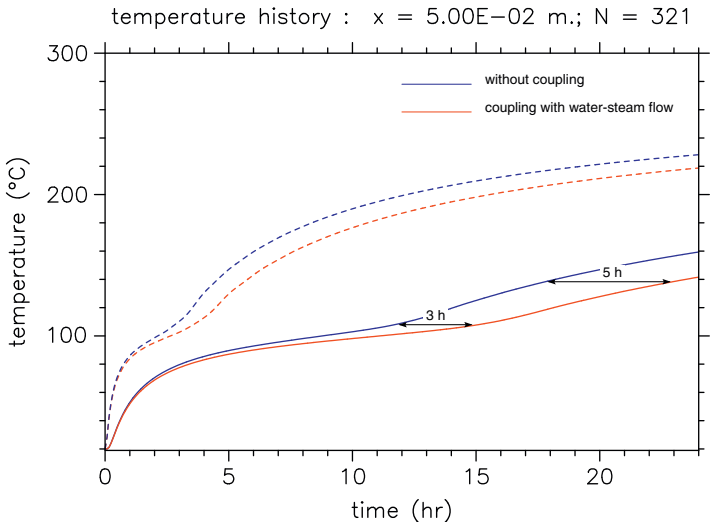

Figure 7. Effects of coupling between heat diffusion with phase change and the water steam flow. Plain curves (resp. dashed curves) represent the temperature histories at the depth 5 cm (resp. 2.5 cm). Taking into account the steam convection introduces a delay in the heating that can reach few hours.

transports energy toward surface. Obviously, the delay is proportional to the heating duration but appears only after the phase-change front. Similarly, the delay is negligible in the wet zone.

9.3. Numerical validations

After focusing on a theoretical and numerical point of view on different ways to solve our system of PDAEs, the validation stage leads us to compare the code results with the experimental ones. Actually, the model has been applied to the famous Stefan problem (melting problem) and has been validated by comparing the numerical results with an existing analytical solution [23]. The experiments deal with non-saturated porous media; hence, we are going to use ϕ as the humidity rate instead of viewing it as the ratio of void as represented in the model described in Section 2. Hence, this will allow us to simulate heat transfer in non-saturated porous media.

DOI: 10.1002/nme

Fluid phase	Capacity $(J/Kg.K)$	Conductivity $(W/m.K)$	Density (Kg/m^3)
Liquid	4.10^3	6.10^{-1}	10^3
Vapor	2.10^3	25.10^{-3}	8.10^{-1}
Porous matrix (clay soil)	13.10^2	756.10^{-3}	15.10^2

Figure 8. Physical properties used for simulations.

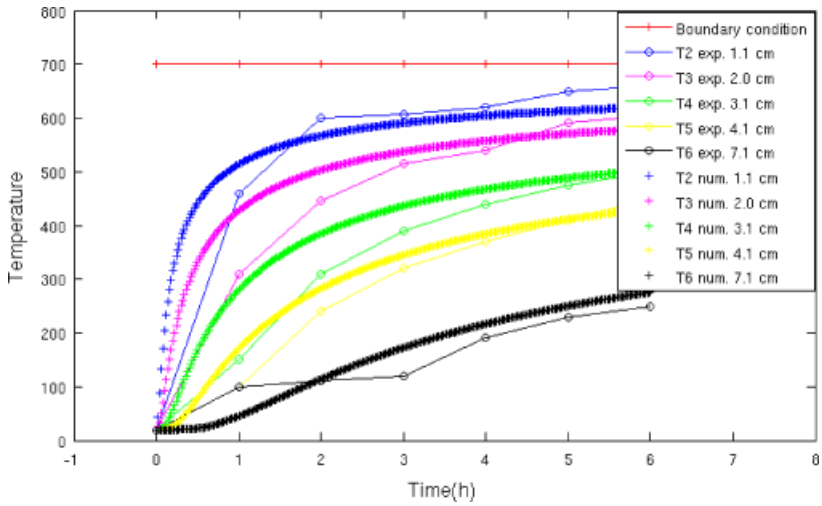

Figure 9. Simulation of the experiment of Laloy and Massard [24] using `DIFFUSE-WC`. The curves show a comparison between numerical results and experimental data.

The physical properties for the fluid phase and the porous matrix used in the simulations are shown in Figure 8. For all cases, we take $L = 2400 \cdot 10^3\,\mathrm{J/kg}$.

As a first validation example, the experiment of Laloy and Massard [24] may be used. This experiment was done on a clay dry soil ($\phi = 0$) from the archaeological site of Etiolles; the temperature at the top of the soil was 700°C. The simulation implied a 2D grid, with 50 points along x and 50 points along depth, temperature interval $\Delta T = 5°\mathrm{C}$ which is the optimal choice to attempt the good accuracy and to avoid the fluctuations [25]. Figure 9 shows the comparison between the simulation and the experiment. The variation of temperature at the depth 7.1 cm is obviously due to some humidity in the soil, as has been also pointed out by Laloy and Massard [24]. As may be observed results compare reasonably well, it may be concluded that, despite the uncertainties coming from the experimental data, the simulations show similar trends and this is an indication that reasonable agreement between replication experiments and simulations may be expected.

The second example of validation is provided considering the water content in the soil. As the aim of this work is to present an application of replication experiments and numerical modeling in the archaeological research, specially the study of archaeological hearths used for cooking and heating, the experiments have been done in Pincevent, near Paris, which was occupied by the ancient hunther-gatherer groups 12.000 BP. The Magdalenian site of Pincevent is located in the valley of the Seine river, approximately 72 km to the south of Paris near Montereau France. The experiments must provide data to validate computational models developed to simulate the heat transfer from the fire to the underlying soil. That is why we choose to realize a controlled experiment using an electrical plate to heat the soil. Thus, the replication consists of heating the surface of the soil using an electrical plate, taking continuous care of its intensity. Also, we put many sensors in the soil at different depths and different positions under the plate (see Figure 10), to measure the temperature distribution in the soil, and we place one sensor at the surface in contact with the plate to measure the plate temperature (see Figure 11). Hence, we determine the

DOI: 10.1002/nme

Figure 10. Sensors are inserted in the soil.

Figure 11. Electrical plate is put on the soil.

Figure 12. Alteration at the surface.

different zones of alterations at the soil surface once the plate is driven away (see Figure 12), and we excavate the hearth to determine the approximate temperature levels reached in the experiments, to mark the changes in coloration due to the thermal alteration and to determine the sensors positions (see Figure 13).

The comparison between numerical results and experimental ones is shown in Figure 14 where the rate of humidity in the soil $\phi = 15\%$ (an estimation that gives a reasonable concordance between numerical and experimental curves) is used in the simulation with a grid of 50×50 nodes. The results show a good agreement between numerical results and measured temperatures. However, the differences between numerical results and experimental ones are due to the incertitude of the thermocouples positions, also due to the approximated properties of the soil. Furthermore, the plateaus shown in this figure are due to the water evaporation in the soil (phase-change problem).

DOI: 10.1002/nme

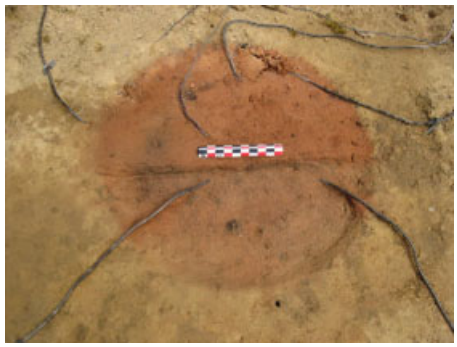

Figure 13. Excavation of the soil.

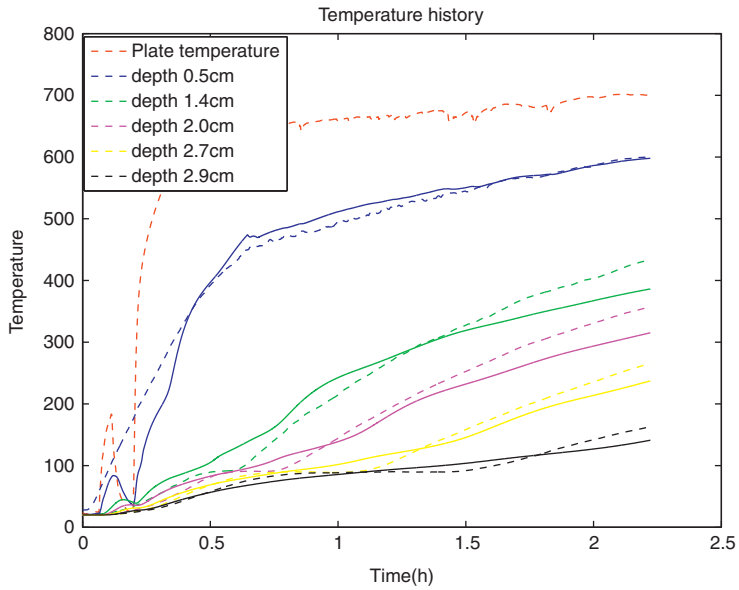

Figure 14. Comparison between numerical results and experimental ones realized on the archaeological hearths at the Pincevent site using an electrical plate. Dashed lines represent experimental data, whereas others are the numerical results obtained by `DIFFUSE-WC`.

The fall in temperature in the dashed magenta curve is due to an error in measures or probably because we moved the sensor during the experiment. The fact that the plateaus obtained by the simulations are not so marked as in the experiments is due to the inherent choice of our model. Figure 15 illustrates the temperature profile in the ground at the end of the experiment.

Other experiments have been done using a real fire as illustrated in Figures 16 and 17. After several hours of continuous burning and keeping a nearly constant mass of fuel, fire was left to extinguish. All along the experiment, temperatures of the fire, ambient conditions, temperature of the soil and wind velocity were recorded. The sampling time was approximately 5 min. A schematic view of one of the experiments that shows the different positions of thermocouples is illustrated in Figure 18 where the used humidity rate was $\phi = 10\%$ (an estimation that gives a reasonable concordance between numerical and experimental curves), and the grid node was 50×50. The comparison between the numerical results and the experimental ones is illustrated in Figure 19, which shows the time evolution of the results as obtained from the code and the experimental measurements. Hence, a reasonable concordance between the replication experiments and the computer results is observed. However, the discrepancies shown between the numerical results and the measured ones specially for thermocouple $T6$ may be caused by the failure of the

DOI: 10.1002/nme

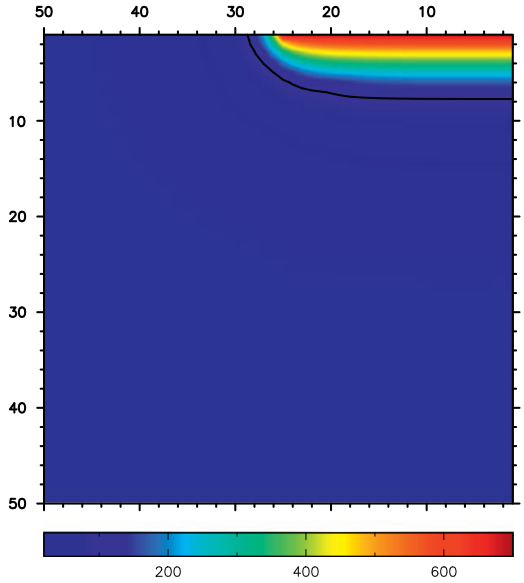

Figure 15. Temperature profile in the 3D axisymmetric case for the experiment with the electrical plate. The black curve represents the phase-change interface position after 2 h of lighting (isotherm at 100°C). Domain size: 50×50 cm.

Figure 16. Real fire used to heat the soil.

initialization for the boundary condition (we are taking the temperature at the center of the fire as a uniform temperature for the uncontrolled bed, which is not the case in reality), or may be due to the uncertainty properties of the porous medium. Moreover, there is the question of weather (fire is sensitive to the wind) that may remain unanswered since the various properties of the experimental conditions are not fully known. It should be pointed out that the temperature history curves presented herein appear quite similar to those reported elsewhere in the literature.

The plateaus at the phase-change temperature observed in Figure 19 are due to the phase-change phenomenon. The water vapor produced at the discontinuous moisture front migrates from the front toward the dry side. Figure 20 shows the temperature profile in the ground. The convective flow is shown by the measured and computed pressure distribution, illustrated in Figure 21, with the velocity in the direction of the negative pressure gradient (see Figure 22). We can see that the highest pressure reached is at the interface level where the evaporation process happens. In this experiment, we are dealing with a medium of small permeability ($K = 10^{-12}\,\mathrm{m}^2$), and so the vapor finds more difficulties to escape from the ground; thus, there is significant variation of the pressure in the soil.

DOI: 10.1002/nme

Figure 17. Alteration of the soil after the experiment.

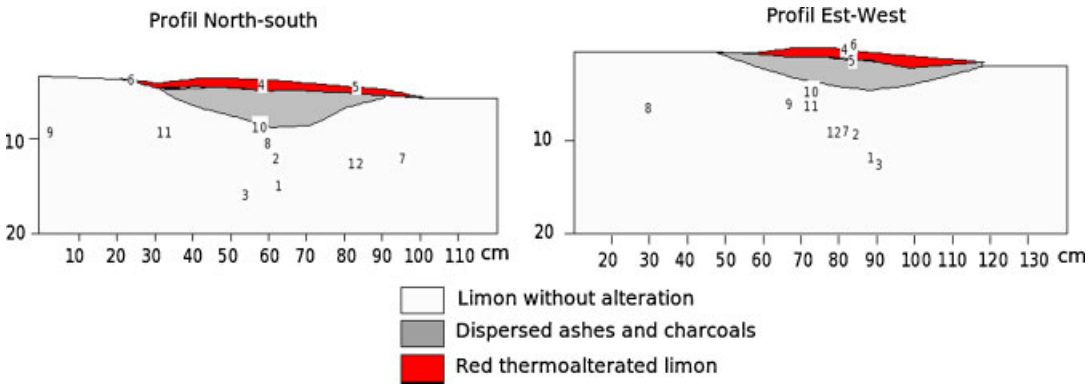

Figure 18. Schematic view of the experiment with the different positions of thermocouples.

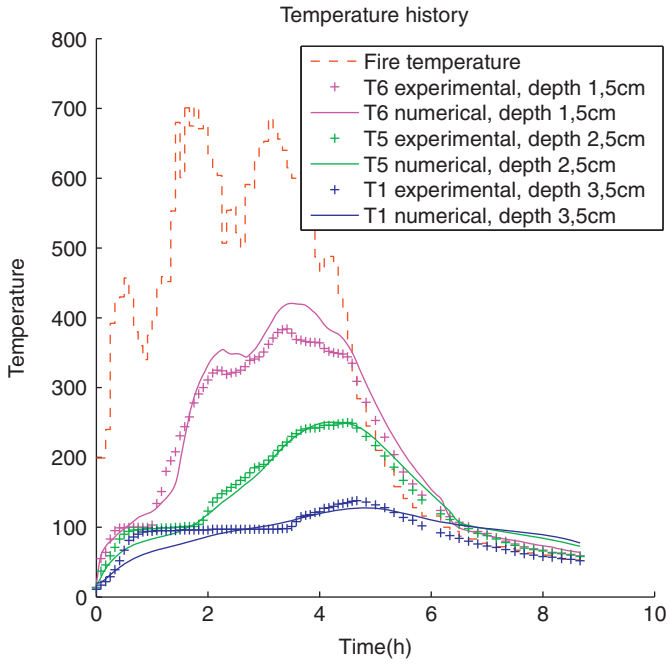

Figure 19. Comparison between numerical results obtained by DIFFUSE-C and experimental ones realized on the archaeological hearths at the Pincevent site. Real fire has been used.

DOI: 10.1002/nme

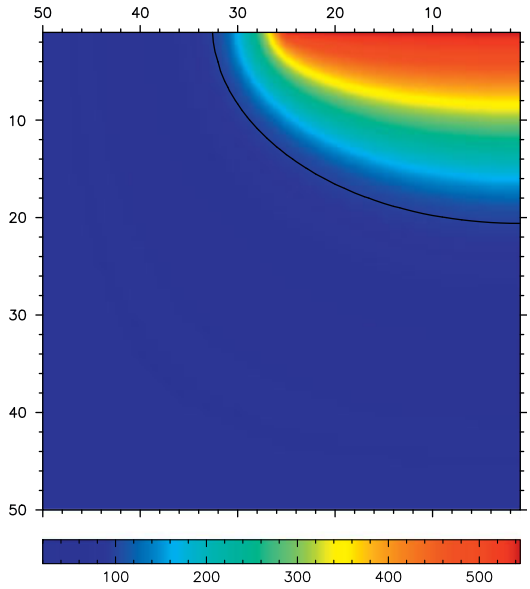

Figure 20. Temperature profile in the ground for the real fire Pincevent experiment. The black curve represents the phase-change interface position (isotherm 100°C) at the end of the lighting. Domain size: 50×50 cm.

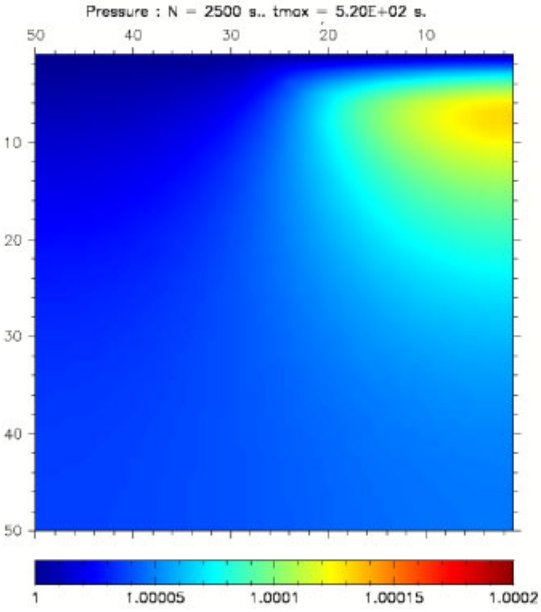

Figure 21. Pressure distributions in the ground. It is due to the gas created at the interface of phase change. Domain size: 50×50 cm.

9.4. Radiation effect

Ferreri and March [26–29] have developed a numerical model in 3D-axisymmetric case called `Pince-eu`, which simulates the heat transfer in saturated porous media. Their code takes into account the phase-change phenomenon and the radiation effect at the surface of the soil, but it neglects the convection effects due to the coupling with the water steam flow. Therefore, in order to study the radiation effect, it seems necessary to compare our model `DIFFUSE-WC` with `Pince-eu`.

DOI: 10.1002/nme

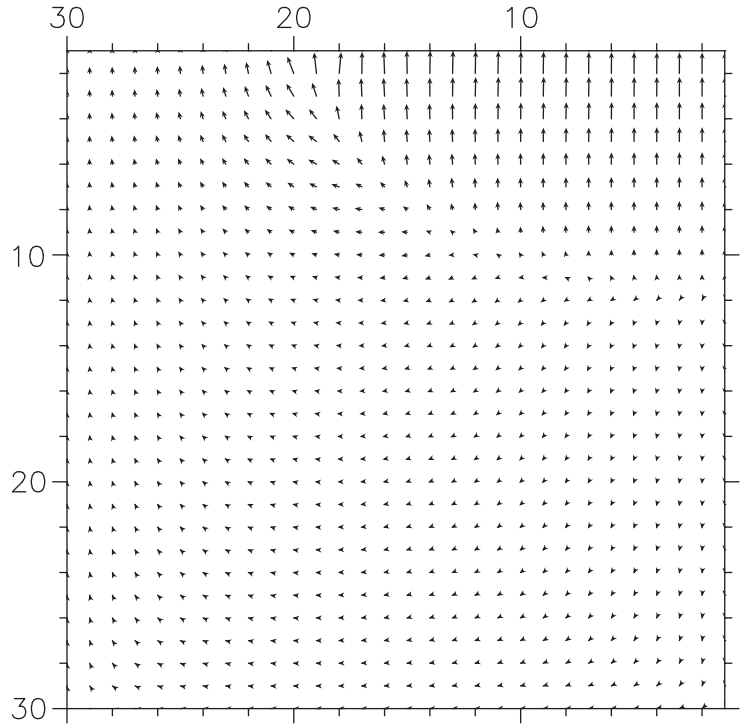

Figure 22. Water steam flow pattern. Domain size: 50×50 cm. Max. velocity: 2.6×10^{-6} m/s.

In fact, `Pince-eu` solves the same physical problem as `DIFFUSE-WC` and in addition it includes the radiation phenomenon that allows to simulate the heat transfer in a bowl occupation, which is not the case in our model.

In fact, the numerical method used in `Pince-eu` is based on the discretization of the Fourier equation using the finite difference method, the coordinate transformations and the apparent capacity method given by Bonacina and Comini [11]. This software is coded in Fortran 77.

To compare the two models (`DIFFUSE-WC` and `Pince-eu`), we simulate the same experience realized at the archaeological site of Pincevent; it is an experience of real fire lighted at the surface of the soil. We used a finite domain of $1\,\text{m} \times 1\,\text{m}$ with a circular fire at the surface with diameter $d = 30\,\text{cm}$. The variable measured temperature at the center of the fire is used as a boundary condition at the surface (we suppose that the temperature at the surface is uniform). The comparison is illustrated in Figure 23 and it shows that the two models reproduce the same behavior. On the other hand, we can see the difference between the results of the two models when cooling starts; this is due to the radiation effect and this is one of the limitations of our model. Otherwise, the big advantage of our code is that it couples the heat diffusion with the water steam flow that has a pronounced effect on the heating curves when dealing with long time fires. Also, the numerical method proposed to solve our model is adapted to the use of unstructured meshes, which is not the case with the method of orthogonal boundary fitted used in `Pince-eu`; this limits the modelization of hearths with complex geometries. For the bowl occupations, the interior boundaries are heated by radiation; hence, it seems interesting to include the radiation effect into our model to modelize such occupations.

10. CONCLUSION

In this paper, we have developed a numerical model that simulates heat diffusion in saturated porous media coupled with the water steam flow problem (due to the creation of vapor when it

DOI: 10.1002/nme

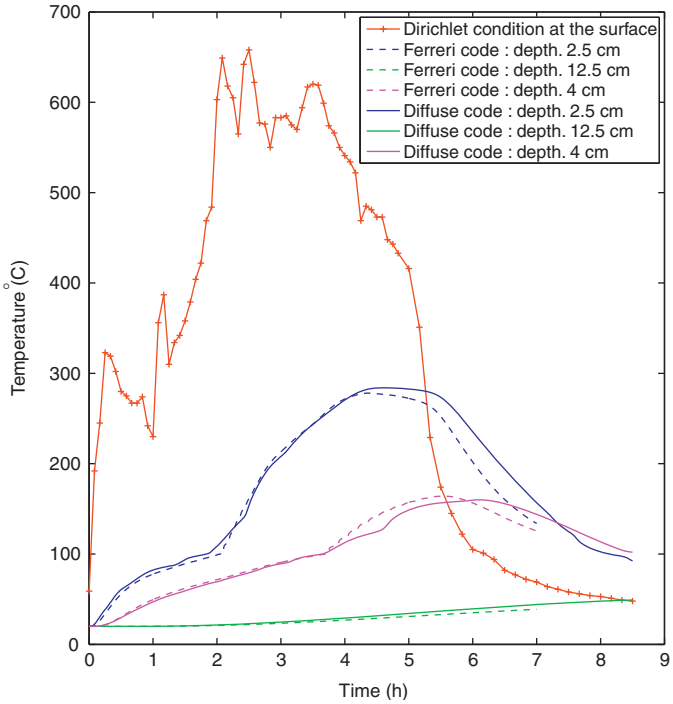

Figure 23. Comparison between our model of heat diffusion with phase change without coupling and `Pince-eu` code.

occurs). We propose a global method based on the AHC method, in order to avoid the tracking of the phase-change interface, and on the use of a DAE solver devoted to handle the coupling between the energy and the water steam flow equations. We use a method of lines to discretize separately in space and time. Actually, due to the strong coupling, this requires to control the time step and the convergence of the Newton iterations. We advocate the use of DAE solvers, which are very efficient in this control, at the price of a larger non-linear system but with the benefit of a better stability.

Numerical results show interesting features concerning the retarding effect of the coupling between heat diffusion and water steam flow; this is due to the convection phenomenon. Obviously, the retarding effect of the water–steam convection depends on the position of the considered point. It occurs mainly in the dry zone, but it is not pronounced in the wet zone. Moreover, this retarding effect occurs more and more later as the position is more and more deeper in the soil. Therefore, as we are looking for the minimal duration of burning based on the alterations of the soil (colors change in the soil corresponding to the temperature $T = 300°C$ when dealing with clay–limon soil), the effect of the convection term is really important and could change fundamentally the interpretation of the results.

Finally, we plan to extend the proposed algorithm to the real 3D case and wish to take into account the radiation effect that is essential to simulate bowl occupations where the edges are heated by radiation also and not only by conduction.

ACKNOWLEDGEMENTS

This work has been done in the frame of ARPHYMAT,[‡] collaboration, with a financial support from the MENR, France. The authors thank Q. Qiong for her participation in the experiments of Pincevent. Also,

[‡]ARchaeology, PHYsics and MAThematics (ARPHYMAT) is an interdisciplinary project involving the three laboratories mentioned in the first page.

DOI: 10.1002/nme

they thank all the archaeologists working at Pincevent, specially the persons in charge of the site for having placed the site of excavation into our disposal.

REFERENCES

1. Muhieddine M. Simulation numérique des structures de combustion préhistoriques. *Ph.D. Report*, Rennes, France, 2009.
2. Cannon J, Hill C. Existence, uniqueness, stability and monotone dependence in a Stefan problem for the heat equation. *Journal of Mathematics and Mechanics* 1967; **17**:1–20.
3. Cannon J, Primicerio M. A two phase Stefan problem with temperature boundary conditions. *Annali di Matematica Pura ed Applicata* 1971; **4**(88):177–192.
4. Bejan A, Kraus AD. *Heat Transfer Hand Book*. Wiley: New York, 2003.
5. Luikov AV. *Analytical Heat Diffusion Theory*. Academic Press: New York, 1968.
6. Pawlow I. Numerical solution of a multidimensional two-phase Stefan problem. *Numerical Functional Analysis and Optimization* 1985; **8**:55–82.
7. Kim CJ, Kaviany M. A numerical method for phase-change problems. *International Journal of Heat and Mass Transfer* 1990; **33**(12):2721–2734.
8. Askar HG. The front-tracking scheme for the one-dimensional freezing problem. *International Journal for Numerical Methods in Engineering* 1987; **24**:859–869.
9. Prapainop R, Maneeratana K. Simulation of ice formation by the finite volume method. *Songklanakarin Journal of Science and Technology* 2004; **26**(1):55–70.
10. Muhieddine M, Canot E. Recursive mesh refinement for vertex centered FVM applied to a 1-d phase-change problem. *FVCA5*. Hermes: Aussois-France, 2008; 601–608.
11. Bonacina C, Comini G. Numerical solution of phase-change problems. *International Journal of Heat and Mass Transfer* 1973; **16**:1825–1832.
12. Comini G, Delgiudice S, Lewis RW, Zeinkiewicz OC. Finite element solution of nonlinear heat conduction problems with special reference to phase change. *International Journal for Numerical Methods in Engineering* 1974; **8**:613–624.
13. Majchrzak E, Mochnaki B, Suchy JS. Identification of substitute thermal capacity of solidifying alloy. *Journal of Theoretical and Applied Mechanics* 2008; **46**(2):257–268.
14. Angirasa A, Peterson GP. Natural convection below a downward facing heated horizontal surface in a fluid-saturated porous medium. *Numerical Heat Transfer* 1998; **34**(3):301–311.
15. Combarnous M, Bories S. Modélisation de la convection d'une couche poreuse horizontale à l'aide d'un coefficient de transfert solide–fluide. *International Journal of Heat and Mass Transfer* 1974; **17**:505–514.
16. Zheng C, Bennett G. *Applied Contaminant Transport Modeling* (2nd edn). Wiley: New York, 2002.
17. Feulvarch E, Bergheau JM, Leblond JB. An implicit finite element algorithm for the simulation of diffusion with phase changes in solids. *International Journal for Numerical Methods in Engineering* 2009; **78**(12):1492–1512.
18. Zheng C, Bennet GD. *Applied Contaminant Transport Modeling* (2nd edn). Wiley-Interscience: New York, 2002.
19. Sboui A, Jaffere J. Discrétisation en temps par sous-domaines pour un problème d'advection en milieux poreux. *ARIMA* (*Revue Africaine de la recherche en informatique et mathématiques appliquées*) 2006; **5**:333–349. Available from: http://www-direction.inria.fr/international/arima/005/pdf/arima00523.pdf.
20. Reichelt M, Shampine L, Kierzenka J. Solving index-1 daes in matlab and simulink. *SIAM* 1999; **41**(3):538–552.
21. Ortega JM, Rheinboldt WC. *Iterative Solution of Nonlinear Equations in Several Variables*. Academic Press: New York, 1970.
22. Dennis JE, Schnabel RB. *Numerical Methods for Unconstrained Optimization and Nonlinear Equations.* Prentice-Hall: NJ, 1983.
23. Muhieddine M, Canot E, March R. Various approaches for solving problems with heat conduction with phase change. *International Journal of Finite Volume Method* 2008; **6**(1).
24. Laloy J, Massard P. Nouvelle méthode thermique d'étude des foyers préhistoriques. *Révue d'Archéométrie* 1984; **8**:33–40.
25. Muhieddine M, Canot E, March R. Numerical solution of a 1-d time dependent phase change problem. *Fifth European Congress on Computational Methods in Applied Sciences and Engineering*, Venise, Italy, 2008.
26. March RJ, Ferreri JC. Sobre el estudio de estructuras de combustion arquelogicas mediante replicationes y modelos numéricos. *Nature et Fonction des foyers préhistoriques*. APRAIF: Nemours, 1987; 59–69.
27. March RJ, Ferreri JC. De modelos numéricos para la inferencia del tiempo de quemado en estructruas de combustion arqueologicas: influencia de parametros. *Actas del TextrmIX Congreso Nacional de Arqueologia Chilena*. Museo National de Historia Natural: Santiago de Chile, Chile, 157–168.
28. March RJ. L'étude des structures de combustion en archéologie : un détour vers l'histoire. *Annales de la Revue Fyssen* 1995; **10**:53–68.
29. Ferreri JC, March RJ. Using numerical models to analyze archaeological simple fires structures. *XIII International Congress of Prehistoric and Protohistoric Sciences*, Colloquia 5, The lower and Middle paleolithic Colloquium, Forli-Italia, 8/14 September 1996; 57–63.

DOI: 10.1002/nme